

# Non-resonant direct $p$ - and $d$ -wave neutron capture by $^{12}\text{C}$

T. Kikuchi<sup>a</sup>, Y. Nagai<sup>a</sup>, T. S. Suzuki<sup>a</sup>, T. Shima<sup>a</sup>, T. Kii<sup>a</sup>, M. Igashira<sup>b</sup>,

A. Mengoni<sup>c,d,e</sup>, and T. Otsuka<sup>c,e</sup>

<sup>a</sup> *Tokyo Institute of Technology, Department of Applied Physics,*

*O-okayama, Meguro, Tokyo 152, Japan*

<sup>b</sup> *Tokyo Institute of Technology, Research Laboratory for Nuclear Reactors,*

*O-okayama, Meguro, Tokyo 152, Japan*

<sup>c</sup> *The Institute of Physical and Chemical Research (RIKEN),*

*Wako, Saitama 351-01, Japan*

<sup>d</sup> *National Institute for New Technologies, Energy and Environment (ENEA),*

*v. Don Fiammelli 2, I-40128 Bologna, Italy*

<sup>e</sup> *The University of Tokyo, Department of Physics,*

*Hongo, Bunkyo, Tokyo 113, Japan*

## Abstract

Discrete  $\gamma$ -rays from the neutron capture state of  $^{13}\text{C}$  to its low-lying bound states have been measured using pulsed neutrons at  $E_n = 550$  keV. The partial capture cross sections have been determined to be  $1.7 \pm 0.5$ ,  $24.2 \pm 1.0$ ,  $2.0 \pm 0.4$  and  $1.0 \pm 0.4$   $\mu\text{b}$  for the ground ( $J^\pi = 1/2^-$ ), first ( $J^\pi = 1/2^+$ ), second ( $J^\pi = 3/2^-$ ) and third ( $J^\pi = 5/2^+$ ) excited states, respectively. From a comparison with theoretical predictions based on the non-resonant direct radiative capture mechanism, we could determine the spectroscopic factor for the  $J^\pi = 1/2^+$  state to be  $0.80 \pm 0.04$ , free from neutron-nucleus interaction ambiguities in the continuum. In addition we have detected the contribution of the non-resonant  $d$ -wave capture component in the partial cross sections

for transitions leading to the  $J^\pi = 1/2^-$  and  $J^\pi = 3/2^-$  states. While the  $s$ -wave capture dominates at  $E_n \leq 100$  keV, the  $d$ -wave component turns out to be very important at higher energies. From the present investigation the  $^{12}\text{C}(n, \gamma)^{13}\text{C}$  reaction rate is obtained for temperatures in the range  $10^7 - 10^{10}$  °K.

## I. INTRODUCTION

An increasing interest has been recently developed around the low energy neutron capture reaction mechanisms induced by light nuclei in view of the importance of the related cross section for the investigation of nuclear structure properties as well as for applications in nuclear astrophysics [1–6]. In fact, it has been recently shown that  $(n, \gamma)$  reactions, together with their time-reversal counterpart, the Coulomb dissociation process, can provide crucial information on the structure of bound-state wave functions in light nuclei. In particular, it has been recently shown [6,7] that the external component of the radial wave function can be extracted from the matrix elements of the electromagnetic E1-operator connecting  $p$ -wave states in the continuum to loosely-bound  $l=0$  orbits (halo states).

On the other hand, neutrons with kinetic energies in the keV-range correspond to the temperature in stars where a variety of capture processes take place ( $1 \text{ keV} = 11.6 \times 10^6 \text{ }^\circ\text{K}$ ). The capture cross sections of medium-mass and heavy nuclei required for the interpretation of various mechanisms of stellar nucleosynthesis have been extensively measured in the course of the last few decades [8,9]. However, fast neutron capture cross sections have been rarely measured for light nuclear targets.

Recently, discrete  $\gamma$ -rays following the neutron capture by light nuclei such as  $^{12}\text{C}$  and  $^{16}\text{O}$  have been successfully measured for incident neutron energies in the keV region [1–3]. It was found that the partial cross section from the capture state of  $^{13}\text{C}$  to the ground state ( $J^\pi = 1/2^-$ ) decreases with increasing neutron energy as expected for  $s$ -wave capture, while the cross sections leading to the first-excited states ( $J^\pi = 1/2^+$ ) in  $^{13}\text{C}$  and  $^{17}\text{O}$  increase with increasing neutron energy. In addition, the capture  $\gamma$ -ray branching ratios markedly favor the transition to these excited states, unlike the observed branching ratios of thermal neutron capture. These new observations indicate the characteristic features of a non-resonant  $p$ -wave direct neutron capture process taking place as will be discussed below.

The discrete  $\gamma$ -ray detection is crucial for studying nuclear structure and reaction mechanisms since the  $\gamma$ -ray carries unique information connecting the capture state and the

low-lying bound states. However, the prompt discrete  $\gamma$ -ray detection for capture events in light nuclei is extremely difficult due to the small cross section expected for light nuclei. As an example, extrapolating the thermal capture cross section of  $^{12}\text{C}$ ,  $\sigma_{n,\gamma}^{th} = 3.53$  mb, with a  $1/v$ -law one obtains  $\sigma_{n,\gamma} = 3.2$   $\mu\text{b}$  at  $E_n = 30$  keV and  $\sigma_{n,\gamma} = 0.8$   $\mu\text{b}$  at  $E_n = 500$  keV. In actual experiments it is difficult to discriminate the weak  $\gamma$ -ray signal from the huge background due to the capture of neutrons scattered and/or thermalized by the collision with various materials in the experimental room. In spite of this, we have recently succeeded to detect discrete  $\gamma$ -rays from the  $^{12}\text{C}(n, \gamma)^{13}\text{C}$  reaction for incident neutron energies in the keV region by developing a highly sensitive discrete  $\gamma$ -ray detection system. We have already reported on the measurement performed at neutron energies up to  $E_n = 200$  keV [2]. Here we report on the results obtained at much higher energy,  $E_n = 550$  keV. From this new experiment and from the theoretical investigation which we will describe below, we have derived the  $^{12}\text{C}(n, \gamma)^{13}\text{C}$  reaction rate for temperatures in the range  $10^7 - 10^{10}$  °K.

## II. THE EXPERIMENT

The experiment was carried out using a prompt discrete  $\gamma$ -ray detection method combined with a pulsed neutron beam. The neutrons were produced by the  $^7\text{Li}(p, n)^7\text{Be}$  reaction using the pulsed proton beam with a pulse width of 1.5 ns, provided by the 3.2 MV Pelletron Accelerator of the Research Laboratory for Nuclear Reactors at the Tokyo Institute of Technology. An average beam current of 12  $\mu\text{A}$  was obtained at a repetition rate of 4 MHz. The neutron energy spectrum was measured by a  $^6\text{Li}$ -glass scintillation counter set at  $9.6^\circ$  with respect to the proton beam direction. An averaged neutron energy spectrum of 550 keV (shown in Fig. 1 after correction for energy dependent efficiency detection) was obtained at the sample position as a consequence of the reaction kinematics. Two samples with a 90 mm diameter, one of natural carbon (C) of reactor grade and one of gold (Au) were placed 19.8 cm away from the Li target at  $0^\circ$  with respect to the proton beam direction. This distance was necessary to separate the  $\gamma$ -ray events caused by the sample from the intense

$\gamma$ -ray flux coming from the  ${}^7\text{Li}(p, \gamma){}^8\text{Be}$  reaction taking place at the neutron target position. The Au sample was used for normalization of the absolute capture cross section since the cross section of Au is known accurately (within an uncertainty of 3% [10]).

The thickness of the C sample was 30 mm. This has been determined so as to balance the reaction yield with the neutron transmission. In fact, with increasing sample thickness the yield increases, but the neutron transmission becomes lower. Therefore, the number of events due to multiple scatterings in the sample increases and the cross section would not be determined accurately.

The prompt  $\gamma$ -rays emitted in the transition from the capture state of  ${}^{13}\text{C}$  to the low-lying states were measured by an anti-Compton NaI(Tl) spectrometer [11] consisting of a central NaI(Tl) detector with a diameter of 6 inches and length of 8 inches and an annular detector with thickness of 3 inches and length of 14 inches. The spectrometer was set at  $125.3^\circ$  with respect to the proton beam direction. Since the NaI(Tl) detector is known to be sensitive to neutrons, we have heavily shielded it using  ${}^6\text{LiH}$ , borated paraffin, Cd sheet and Pb. Using the specially designed spectrometer together with the pulsed neutron beam we could measure discrete  $\gamma$ -rays emitted from a neutron capture state with cross sections as small as  $\approx 10 \mu\text{b}$  at 30 keV. The use of a pulsed neutron beam was crucial not only to determine the neutron energies (by TOF method) but also to discriminate the capture events due to the high energy neutrons from those arising from scattered and/or thermalized ones.

It should be noted that when the neutron energy is as low as 30 keV, the neutrons produced at the neutron target position are emitted within a narrow cone with respect to the proton beam direction. However, when the energy is of the order of 500 keV, the cone aperture becomes large and the neutrons can be scattered and/or directly captured by various materials near the NaI(Tl) detector, producing background. Since there were materials containing carbon atoms in the shield of the NaI(Tl) spectrometer (for example borated paraffin), we made special efforts to reduce these background events [12].

The TOF spectrum measured by the NaI(Tl) spectrometer for the Au sample is shown

in Fig. 2. The sharp peak at channel 440 and the broad one at channel 380 are due to the  ${}^7\text{Li}(p, \gamma){}^8\text{Be}$  and to the  ${}^{197}\text{Au}(n, \gamma){}^{198}\text{Au}$  reactions, respectively. The foreground (FG) and background (BG) spectra for the  ${}^{12}\text{C}(n, \gamma){}^{13}\text{C}$  reaction are shown in Fig. 3. They have been obtained by putting the gates on F- and B-regions in the TOF spectrum shown in Fig. 2. The background subtracted (BS) spectrum is shown in Fig. 4.

The  $\gamma$ -ray energy calibration curve was made using the 1.461 and 2.615 MeV  $\gamma$ -rays from the decays of natural radioactivities of  ${}^{40}\text{K}$  and  ${}^{208}\text{Tl}$ , respectively. In addition, several  $\gamma$ -rays from the  ${}^{56}\text{Fe}(n, \gamma){}^{57}\text{Fe}$  reaction (iron was used to cover the NaI(Tl) spectrometer) induced by thermal neutrons have been used for this purpose [13]. These neutrons were produced by the collision of the incident neutron beam with various materials in the experimental room.

The continuum background in the BS spectrum was considered to be mainly due to the high energy (up to 17 MeV)  $\gamma$ -rays arising from the  ${}^7\text{Li}(p, \gamma){}^8\text{Be}$  reaction at the Li target position. In fact, this background level increased as the gate position in the TOF spectrum was shifted closer to the peak of the  ${}^7\text{Li}(p, \gamma){}^8\text{Be}$  reaction. Hence we measured a  $\gamma$ -ray spectrum without the C sample in order to subtract the continuum background.

The net spectrum, free from the continuum part, is shown in Fig. 5. Two intense peaks at 2.37 and 3.09 MeV can be seen. They arise from the  $\gamma$ -ray cascade originating from the capture state of  ${}^{13}\text{C}$  leading to the ground state via the excited state at 3.09 MeV ( $J^\pi = 1/2^+$ ). The peak width of the 2.37 MeV  $\gamma$ -ray is larger than that of the 3.09 MeV because of the additional contribution of the energy spread of the incident neutrons in the latter transition. The small peaks at 5.46, 3.85 and 3.68 MeV are due to the  $\gamma$ -rays originating from the capture state, the third- and the second-excited states respectively decaying to the ground state (see a partial level scheme of  ${}^{13}\text{C}$  in Fig. 6). It should be mentioned here that the latter two  $\gamma$ -rays were not observed clearly in the previous experiment at  $E_n \leq 200$  keV [2].

The intensities of these  $\gamma$ -rays were analyzed by the stripping method using a response function obtained experimentally [11]. The  $\gamma$ -ray relative intensities thus obtained are compared with those generated by thermal neutrons in Fig. 6. It is worthwhile to note here that

the  $\gamma$ -ray strength from the capture state feeding directly the first excited state in  $^{13}\text{C}$  is large for 550 keV neutrons, whereas for thermal neutrons the largest strength is observed for the transition leading directly to the ground state [14]. The  $\gamma$ -ray for the transition leading to the third excited state was identified for the first time for incident neutron energies of 550 keV by the 3.85 MeV  $\gamma$ -ray, as discussed above.

Since the thermal capture proceeds only by  $s$ -wave neutrons, the strongest transition from the capture state to the ground state is an E1 transition. Assuming the same E1 character for the transition leading to the first excited state, the capture process must proceed via  $p$ -wave neutron capture. Among other things it follows that, because of the E1 character and because the measurement is performed at  $125.3^\circ$ , where the second Legendre polynomial is zero, the observed intensity represents the angle-integrated value.

The partial capture cross section  $\sigma_f$  for the  $^{12}\text{C}(n, \gamma)^{13}\text{C}$  reaction feeding a low-lying state ( $f$ ) is given by using the  $\gamma$ -ray yield  $Y_{\gamma,f}$  as

$$\sigma_f = F \frac{(\phi)_{Au}}{(\phi)_C} \frac{(r^2 n)_{Au}}{(r^2 n)_C} \frac{Y_{\gamma,f}(C)}{Y_{\gamma,f}(Au)} \sigma(Au) \quad (1)$$

with

$$F = \frac{(C_{nm} C_{ns} C_{\gamma a} C_{fs})_{Au}}{(C_{nm} C_{ns} C_{\gamma a} C_{fs})_C}. \quad (2)$$

Here,  $F$  is the correction factor defined in Eq. 2 and  $\phi$  is the neutron yield, respectively.  $r$  and  $n$  are the radius (in cm) and thickness (atoms/barn) of the sample.  $Y_\gamma(Au)$  and  $\sigma(Au)$  are the  $\gamma$ -ray yield and the absolute capture cross section of Au, respectively. The correction factors for neutron multiple scattering effects, for the shielding of the incident neutrons in the sample, for the  $\gamma$ -ray absorbed by the sample and for the finite size of the sample are indicated by  $C_{nm}$ ,  $C_{ns}$ ,  $C_{\gamma a}$  and  $C_{fs}$  respectively. The factors  $C_{nm}$  and  $C_{ns}$  were calculated by a Monte-Carlo code, TIME-MULTI [15] and  $C_{\gamma a}$  and  $C_{fs}$  were also estimated using a Monte-Carlo method. These correction factors are given in Table 1. In calculating the correction factors, both the elastic and the capture reaction processes have been considered as main sources of neutron attenuation. Hence, the coefficient  $C_{nm}$  may differ for  $s$ - and for  $p$ -wave neutrons [15].

### III. RESULTS AND COMPARISON WITH DRC MODEL CALCULATION

The final results for the partial capture cross sections for the transitions leading to the ground, first, second and third excited states in the  $^{12}\text{C}(n, \gamma)^{13}\text{C}$  reaction are given in Table 2. In Fig. 7 we show the present results together with the results of the previous measurement performed at incident neutron energies comprised between 10 and 200 keV. A comparison is made with calculations based on the non-resonant  $s$ -,  $p$ - and  $d$ -wave DRC [6] whose description we will briefly summarize here.

#### A. DRC model calculation

It has been recently shown that while the DRC process of incident  $s$ -wave neutrons captured into bound  $l=1$  orbits is very sensitive to the neutron-nucleus interaction in the continuum, the matrix elements for E1 transitions (hence the cross section) for incident  $p$ -wave neutron capture, leading to the bound  $l=0$  or  $l=2$  orbits are insensitive to this interaction [6]. This can be intuitively understood by simply reminding that the  $p$ -wave neutron collision at low energies is essentially peripheral and therefore unaffected by the neutron-nucleus potential. Consequently, since the basic information on the  $p$ -wave neutron capture process is carried by the structure of the bound-state, its spectroscopic factor,  $S_b$ , can be derived from the measured capture cross section.

To show this let us remind that, for an E1 transition, the DRC cross section of incident neutrons with energy  $E_n$  is given by

$$\sigma_{n,\gamma} = \frac{16\pi}{9\hbar} k_\gamma^3 \bar{e}^2 |Q_{c \rightarrow b}^{(E1)}|^2 \quad (3)$$

Here,  $k_\gamma = \epsilon_\gamma/\hbar c$  is the  $\gamma$ -ray wave number for a transition with emission energy  $\epsilon_\gamma$  and  $\bar{e} = -Z/A$  is the E1 effective charge for a neutron. All the quantum numbers necessary to uniquely define the initial and the final states have been lumped into the notation  $c$  and  $b$ , respectively. The matrix elements for the dipole operator  $\hat{T}^{E1}$  can be decomposed into the products of three terms



$$Q_{c \rightarrow b}^{(E1)} = \langle \Psi_b | \hat{T}^{E1} | \Psi_c \rangle \equiv \sqrt{S_b} \mathcal{I}_{c,b} A_{c,b}. \quad (4)$$

We have indicated with  $A_{c,b}$  the angular coupling part (including orbital and spin coupling coefficients [6]) and with  $\mathcal{I}_{c,b}$  the radial part of the transition matrix elements. The entrance channel wave function (the spin component is omitted in the following)

$$\Psi_{lm}(\mathbf{r}) \equiv w_l(r) \frac{Y_{l,m}(\theta, \phi)}{rv^{1/2}} = \frac{i\sqrt{\pi}}{k} \sqrt{2l+1} i^l [I_l - U_l O_l] \frac{Y_{l,m}(\theta, \phi)}{rv^{1/2}} \quad (5)$$

where

$$I_l \sim \exp(-ikr + \frac{1}{2}il\pi) \quad \text{and} \quad O_l \sim \exp(+ikr - \frac{1}{2}il\pi) \quad (6)$$

may be simply replaced by the  $l=1$  component of the partial wave decomposition of a plane-wave in the incident channel

$$w_{l_c=1}(r) = \frac{(2i)\sqrt{3\pi}}{k} kr j_1(kr). \quad (7)$$

Here,  $j_1(kr)$  is a spherical Bessel function,  $k = \sqrt{2\mu E_n}/\hbar c$  is the wave number corresponding to the incoming neutron energy  $E_n$  and reduced mass  $\mu$ . This ansatz is equivalent to assuming  $U_l \equiv 1$  for all  $l$ . In the more general situation in which the neutron-nucleus interaction in the continuum appreciably perturbs the scattering channel wave function, the collision matrix  $U_l$  can be evaluated numerically using some (optical) model potential. The scattering matrix is related to the optical model phase-shift simply by  $U_l = \exp(2i\delta_l^{opt})$ .

The radial part of the overlap integral

$$\mathcal{I}_{l_c l_b} \equiv \int_0^\infty u_{l_b}(r) r w_{l_c}(r) dr = i\sqrt{12\pi} \int_0^\infty j_1(kr) r^2 u_{l_b}(r) dr \quad (8)$$

can be easily evaluated numerically for any given single-particle radial wave function of the final state, leaving the factor  $S_b$  as the only quantity in Eq. 4 to be determined by the experiment. The accuracy of  $S_b$  thus determined depends on the reliability of the final state wave function and on the accuracy of the measured cross section.

The standard method to calculate this wave function is to use a single-particle model potential, for example a Woods-Saxon potential of type

$$V(r) = \frac{-V_0}{1 + \exp [(r - R)/a]} \quad (9)$$

and solve the bound-state problem for given parameters  $R$ ,  $V_0$ , and  $a$ . The depth of the potential well,  $V_0$ , can be adjusted to reproduce the binding energy. We have adopted this procedure in our calculation assuming the following geometrical parameters for the potential:  $R = 2.86$  fm (corresponding to  $r_0 = 1.25$  fm in  $R = r_0 A^{1/3}$ ) and  $a = 0.65$  fm. A spin-orbit coupling potential with strength  $V_{so} = 6.5$  MeV was added in the case of  $p$ - and  $d$ -orbit calculation. A well-depth  $V_0 = 57.5$  MeV is obtained for a binding energy of 1.86 MeV relative to the  $J^\pi = 1/2^+$  state in  $^{13}\text{C}$  at 3.09 MeV.

These parameters are slightly different from the parameters used in the reference [6]. The resulting DRC cross section calculations obtained using this set of parameters differ from the previous set of calculations by less than 5%. This set has been adopted in order to compare the DRC calculation with the distorted waves Born approximation (DWBA) employed in the analysis of the  $(d, p)$  reaction, used to determine the spectroscopic factors of the bound states of  $^{13}\text{C}$  [16].

The measured cross sections at  $E_n = 550$  keV agree well with the calculation based on the non-resonant DRC mechanism, as was already shown in the low energy region analysis [6]. The results are shown in Table II and Fig. 7. Here we confirm the interpretation of the DRC process and we extend it to higher energy.

From the measured cross section leading to the  $J^\pi = 1/2^+$  state we can derive the spectroscopic factor for the  $|^{12}\text{C}(0^+) \otimes (\nu 2s_{1/2})_{1/2^+} >$  configuration of this state. The spectroscopic factor turns out to be  $S_b = 0.80$ , to be compared with the value derived from the  $(d, p)$  transfer reaction,  $S_b = 0.65$  [16].

In general, a 20% uncertainty in the spectroscopic factor determined from  $(d, p)$  transfer reaction is not uncommon. This uncertainty comes from various factors, including the optical model-dependence of DWBA calculations, usually adopted in transfer reaction analysis. In our case, this uncertainty is removed leaving the geometrical parameters of the bound-state Woods-Saxon potential as the only model-dependent uncertainty. This model dependency

cannot be removed as it is inherent to the definition of spectroscopic factor of a single-particle configuration, such as the  $|^{12}\text{C}(0^+) \otimes (\nu 2s_{1/2})_{1/2^+} \rangle$ , involved in the present case.

Assuming the experimental uncertainty of the measured capture cross section at 550 keV (5%) as the only uncertainty, our analysis results in  $S_b = 0.80 \pm 0.04$  for the  $J^\pi = 1/2^+$  state in  $^{13}\text{C}$ .

The same procedure could be applied to the other transition, the one leading to the  $J^\pi = 5/2^+$  state of  $^{13}\text{C}$  at 3.85 MeV. However, the measured capture cross section leading to this state suffers from large uncertainty and a meaningful determination of the spectroscopic factor for this transition cannot be performed at present.

In the case of the negative-parity states (ground and second excited states of  $^{13}\text{C}$ ), the uncertainty deriving from the assumed model potential used to calculate the collision matrix of the scattering channel does not allow for a determination of the spectroscopic factor with a better accuracy than that obtained by the  $(d, p)$  analysis. This can be easily seen in Fig. 7 where a calculation performed using a simple plane-wave in the incident channel results in a capture cross section two order of magnitude larger than the experimental values.

In our calculations we have adopted the values of  $S_b$  derived from the  $(d, p)$  reaction [16] for the two negative-parity states in  $^{13}\text{C}$ . Still, we would like to stress here that using the same potential parameters obtained to reproduce the bound state at 3.09 MeV in calculating the collision matrix for  $s$ - and  $d$ -waves, we have obtained a very good agreement with the measured capture cross section in the whole energy range. The calculated thermal ( $E_n = 0.0253$  eV) capture cross section, due to these two transitions turns out to be  $\sigma_{n,\gamma}^{th} = 3.15$  mb, to be compared with the experimental  $\sigma_{n,\gamma}^{th} = 3.53 \pm 0.07$  mb [17]. Our interaction is also able to reproduce the thermal scattering radius  $R' = 6.45$  fm, to be compared with the experimental  $R' = 6.3 \pm 0.1$  fm [17]. These results can be considered satisfying as the sensitiveness of the matrix elements to the potential employed to calculate the collision matrix  $U_{l=0}$  and the uncertainty in the spectroscopic factors do not generally allow for better accuracy.

From the data shown in Fig. 7 one can clearly see the onset of the capture of  $d$ -wave

neutrons. In fact, for incident energies up to  $\approx 100$  keV, the  $s$ -wave component of the incident channel wave function is clearly dominant. For higher energies and in particular around 500 keV, the contribution of this higher-order partial wave becomes dominant. To date, this is the first observation of the onset of DRC  $d$ -wave neutron capture.

Finally, it should be added that, in general the presence of resonances near the threshold can make it difficult to compare the measured cross sections with the DRC calculation, due to the possible interference effects between the resonant and the DRC processes. In the  $^{12}\text{C}(n, \gamma)^{13}\text{C}$  reaction, however, the nearest resonance state is rather high, at 2.08 MeV ( $E_n = 2.25$  MeV) with a narrow  $\Gamma = 8 \pm 2$  keV width [17]. Thus, we could deduce the reaction mechanism and nuclear structure information more in detail using neutrons of  $E_n$  between 100 keV to 1 MeV, without worrying about possible interference effects.

### B. $(n, \gamma)$ reaction rate calculation

Using the present results just described we can deduce the  $^{12}\text{C}(n, \gamma)^{13}\text{C}$  reaction rate. This reaction rate is important for several applications in nuclear astrophysics, including the studies of inhomogeneous big-bang models [18], the nucleosynthesis of heavy elements through the  $s$ -process [19] and  $r$ -process [20]. The Maxwellian averaged neutron capture cross section for a temperature  $T$  ( $k$  is the Boltzmann constant), is given by

$$\frac{\langle \sigma v \rangle_{kT}}{v_T} = \frac{2}{\sqrt{\pi}} \frac{1}{(kT)^2} \int_0^\infty E \sigma_{n,\gamma}(E) e^{-E/kT} dE \quad (10)$$

where  $v_T = (2kT/\mu)^{1/2}$  is the velocity corresponding to the thermal energy  $kT$ . A short-hand notation for this quantity often adopted is  $\langle \sigma \rangle_{kT}$ . Indicating with  $\langle \sigma \rangle_{kT}^s$ ,  $\langle \sigma \rangle_{kT}^p$  and  $\langle \sigma \rangle_{kT}^d$  the respective components of the total capture cross section due to incident  $s$ -,  $p$ - and  $d$ -waves, we obtain

$$\langle \sigma \rangle_{kT}^s = \frac{17.3}{\sqrt{kT}}, \quad \langle \sigma \rangle_{kT}^p = 2.01 \sqrt{kT} \quad \text{and} \quad \langle \sigma \rangle_{kT}^d = 6.0 \times 10^{-4} (kT)^{3/2} \quad (11)$$

where the cross sections are in units of  $\mu\text{b}$  when  $kT$  is in units of keV. The  $s$ -wave component has been multiplied by a factor of 1.12 to take into account the discrepancy between the

calculated and experimental thermal cross section (see above).

The resulting reaction rate is

$$\begin{aligned}
 N_A \langle \sigma v \rangle &= 2.753 \times 10^7 \sqrt{kT} \langle \sigma \rangle_{kT} \\
 &= 476.0 \quad + \quad 4765.2 T_9 \quad + \quad 122.5 T_9^2 \quad \text{cm}^3 \text{ mole}^{-1} \text{ sec}^{-1}.
 \end{aligned}
 \tag{12}$$

The usual notation,  $T_9$ , for the temperature in units of  $10^9$  °K and  $N_A$  for the Avogadro constant has been adopted. To show the relevance of the present result in comparison with the previously adopted rate we show in Fig. 8 a comparison of the reaction rates responsible for the  $^{12}\text{C}$  processing for temperatures ranging from  $10^7$  to  $10^{10}$  °K. All the reaction rates, except for our present calculation, have been obtained from the Nuclear Astrophysics Data service [21], mainly adopting the rates of Caughlan and Fowler [22]. It can be seen that the inclusion of the  $p$ -wave component in the capture cross section, resulting in a linear increase of the reaction rate with temperature, makes the neutron capture competing and in most cases exceeding the other processing mechanisms for temperatures of the full range. The consequences of this result on stellar as well as on the big-bang nucleosynthesis modeling is presently under investigation.

#### IV. CONCLUSION

The present work demonstrates clearly the important rôle of prompt discrete  $\gamma$ -ray detection technique using a high resolution NaI(Tl) spectrometer for understanding nuclear structure properties and capture reaction mechanisms. We succeeded for the first time to measure the partial cross sections from the  $^{12}\text{C}(n, \gamma)^{13}\text{C}$  reaction at  $E_n = 550$  keV. By comparing the measured values with a calculation based on a non-resonant DRC model with various partial wave components, we have been able to determine the spectroscopic factor for the  $J^\pi = 1/2^+$  3.09 MeV state in  $^{13}\text{C}$ , reliably. In addition we have unambiguously identified the onset of the  $d$ -wave neutron capture for incident neutron energies above 100 keV. The reaction rate for the  $^{12}\text{C}(n, \gamma)^{13}\text{C}$  reaction obtained by our work differs substantially

from the values adopted so far, producing interesting consequences on the astrophysical applications of our results.

We acknowledge fruitful discussions with M. Ishihara, H. Ohnuma and M. Hashimoto. This work was supported by a grant-in-aid for Specially Promoted Research of the Japan Ministry of Education, Science, Sports and Culture and partly by a grant-in-aid for Scientific Research on Priority Areas.

## REFERENCES

- [1] Y. Nagai, M. Igashira, K. Takeda, N. Mukai, S. Motoyama, F. Uesawa, H. Kitazawa, and T. Fukuda, *Ap. J.* **372** (1991) 683.
- [2] T. Ohsaki, Y. Nagai, M. Igashira, T. Shima, K. Takeda, S. Seino, and T. Irie, *Ap. J.* **422** (1994) 912.
- [3] M. Igashira, Y. Nagai, K. Masuda, T. Ohsaki, and H. Kitazawa, *Ap. J.* **441** (1995) L89.
- [4] Y. K. Ho, H. Kitazawa, and M. Igashira, *Phys. Rev. C* **44** (1991) 1148.
- [5] T. Otsuka, M. Ishihara, N. Fukunishi, T. Nakamura, and M. Yokoyama, *Phys. Rev. C* **49** (1994) R2289.
- [6] A. Mengoni, T. Otsuka, and M. Ishihara, *Phys. Rev. C* **52** (1995) R2334.
- [7] A. Mengoni, T. Otsuka, T. Nakamura, and M. Ishihara, *Proc. Int. Symp. "Capture gamma-ray Spectroscopy and Related Topics"*, G. Molnar Ed., Springer Verlag, in press (1997).
- [8] R. L. Macklin, and J. H. Gibbons, *Rev. Mod. Phys.* **37** (1965) 166.
- [9] F. Käppeller, H. Beer, and K. Wisshak, *Rep. Prog. Phys.* **52** (1989) 945.
- [10] ENDF/B-VI, data file for  $^{197}\text{Au}$  (Mat=7925), evaluated by S. F. Mughabghab.
- [11] M. Igashira, K. Tanaka, and K. Masuda in *Proc. 8th. Int. Symp. on Capture Gamma-ray Spectroscopy and related Topics*, Fribourg, Switzerland, J. Kern Ed., (World Scientific, Singapore, 1994) pag. 992.
- [12] Y. Nagai, *et al.*, *Phys. Rev. C* (1997) in press.
- [13] J. R. Bird, B. J. Allen, I. Bergquist, and J. A. Biggerstaff, *Nuclear Data Tables* **11** (1973) 433.
- [14] F. Ajzenberg-Selove, *Nucl. Phys. A* **523** (1991) 1.

- [15] K. Senoo, Y. Nagai, T. Shima, T. Ohsaki, and M. Igashira, *Nucl. Instr. Meth.* **A339** (1994) 556.
- [16] H. Ohnuma *et al.*, *Nucl. Phys.* **A448** (1985) 205.
- [17] S. F. Mughabghab, M. Divadeenam, and N. E. Holden, *Neutron Cross Sections* (Academic, New York, 1981), Vol. 1.
- [18] T. Kajino, *Nucl. Phys.* **A588** (1995), 339c.
- [19] C. M. Raiteri, R. Gallino, M. Busso, D. Neuberberg, and F. Käppeler, *Ap. J.* **419** (1993), 207; R. Gallino, *private communication* (1996).
- [20] W. M. Howard, S. Goriely, M. Rayet, and M. Arnould, *Ap. J.* **417** (1993), 713.
- [21] Nuclear Astrophysics Data Service, <http://isotopes.lbl.gov/isotopes/astro.html>.
- [22] G.R. Caughlan, and W.A. Fowler, *Atomic Data and Nuclear Data Tables* **40** (1988) 283.



## FIGURES

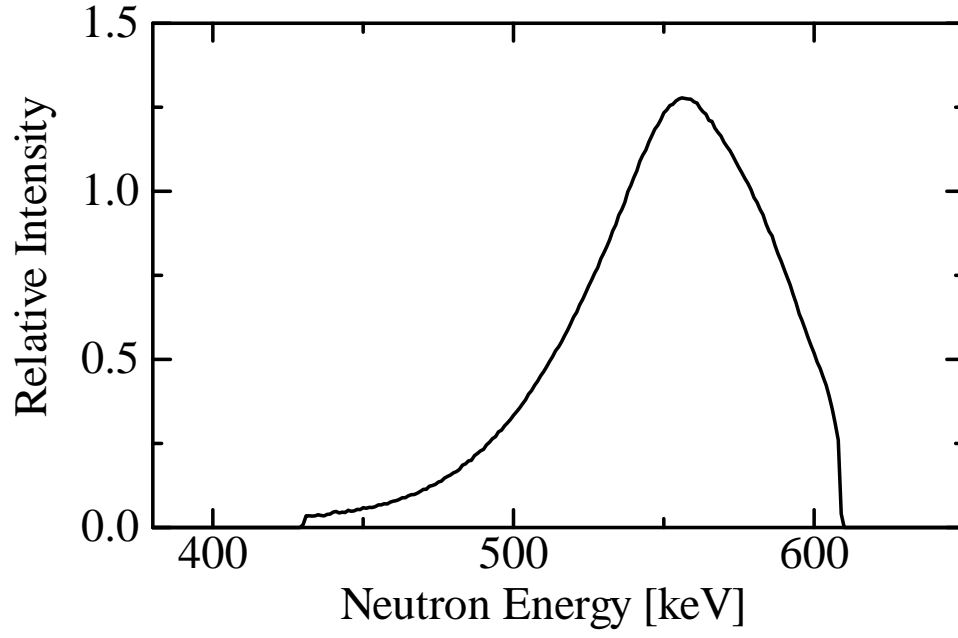


FIG. 1. Neutron energy spectrum measured by a  $^6\text{Li}$ -glass scintillation counter with a TOF method. The spectrum has been corrected for the energy-dependent neutron detection efficiency of the  $^6\text{Li}$ -glass.

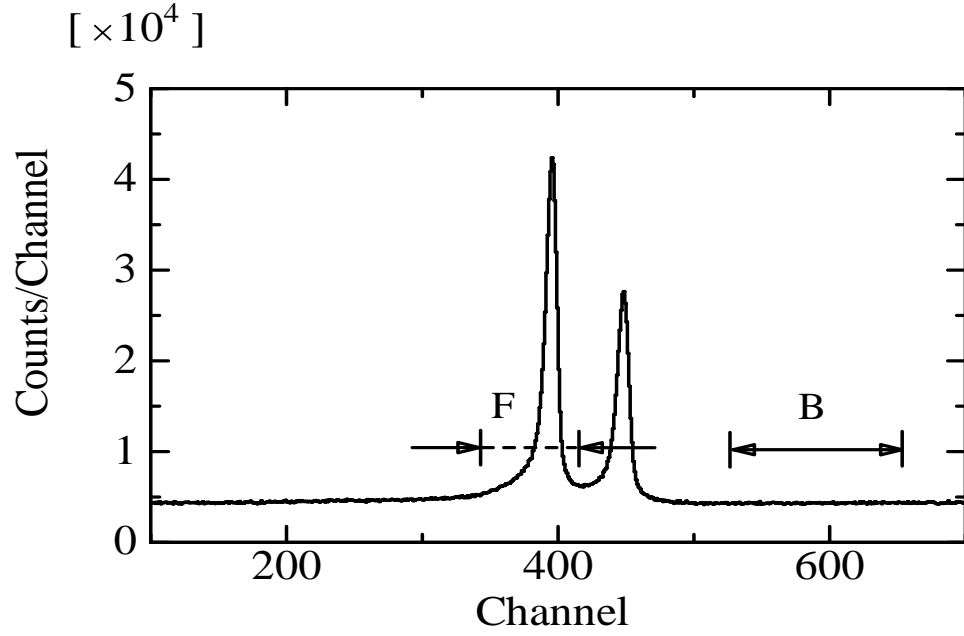


FIG. 2. Time-of-flight spectrum measured by the NaI(Tl) detector for the Au sample. The sharp peak at channel 440 is due to the  $\gamma$ -ray from the  ${}^7\text{Li}(p,\gamma){}^8\text{Be}$  reaction. The regions F and B were chosen to obtain the foreground and background  $\gamma$ -ray spectra, respectively (see text).

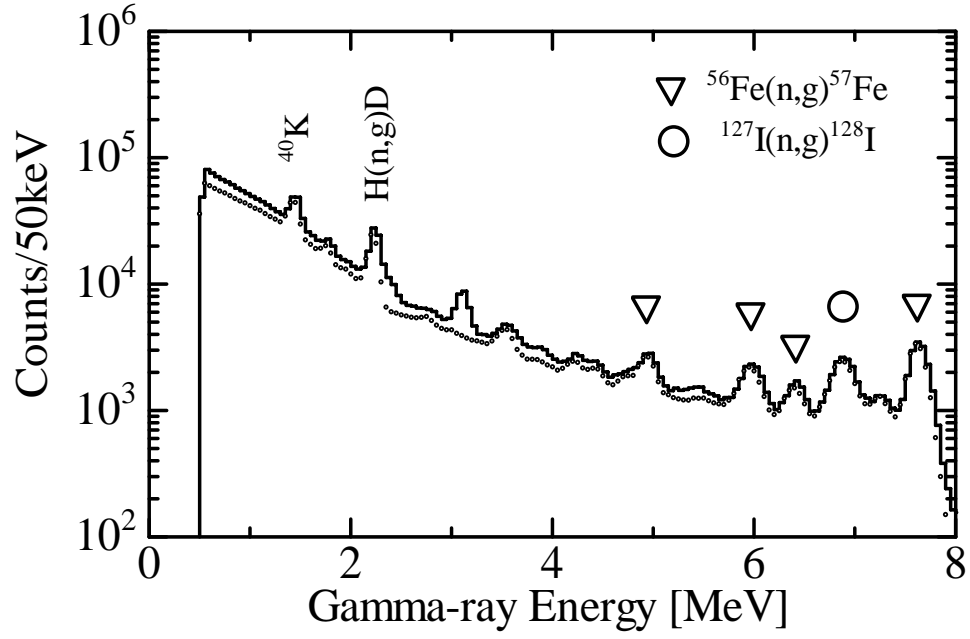


FIG. 3. Foreground (solid line) and background (dotted line)  $\gamma$ -ray spectra for the  $^{12}\text{C}(\text{n},\gamma)^{13}\text{C}$ . Iron was used to cover the NaI(Tl) spectrometer.

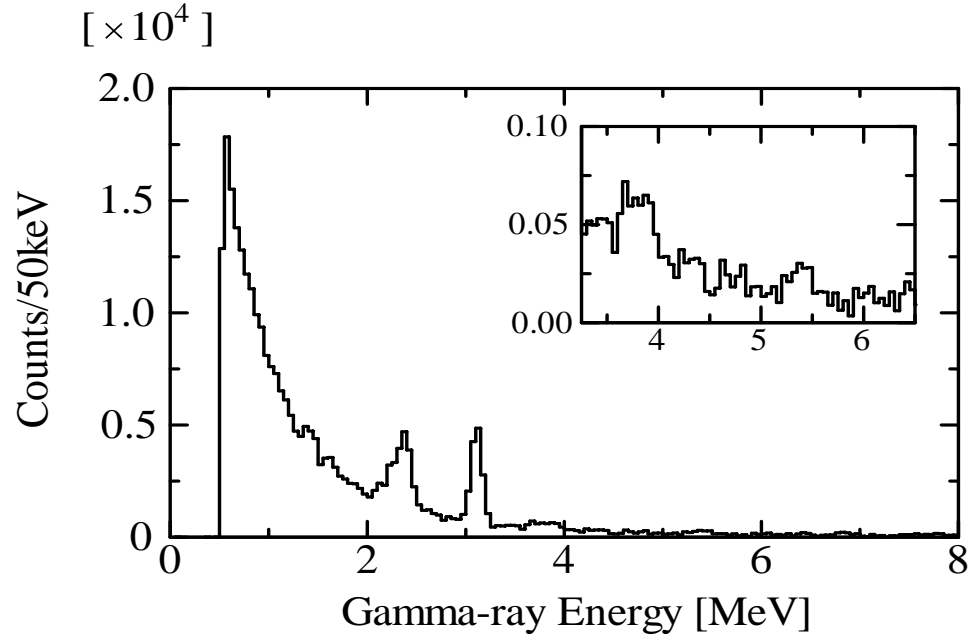


FIG. 4. Background subtracted  $\gamma$ -ray spectra for the  $^{12}\text{C}(n, \gamma)^{13}\text{C}$  reaction.

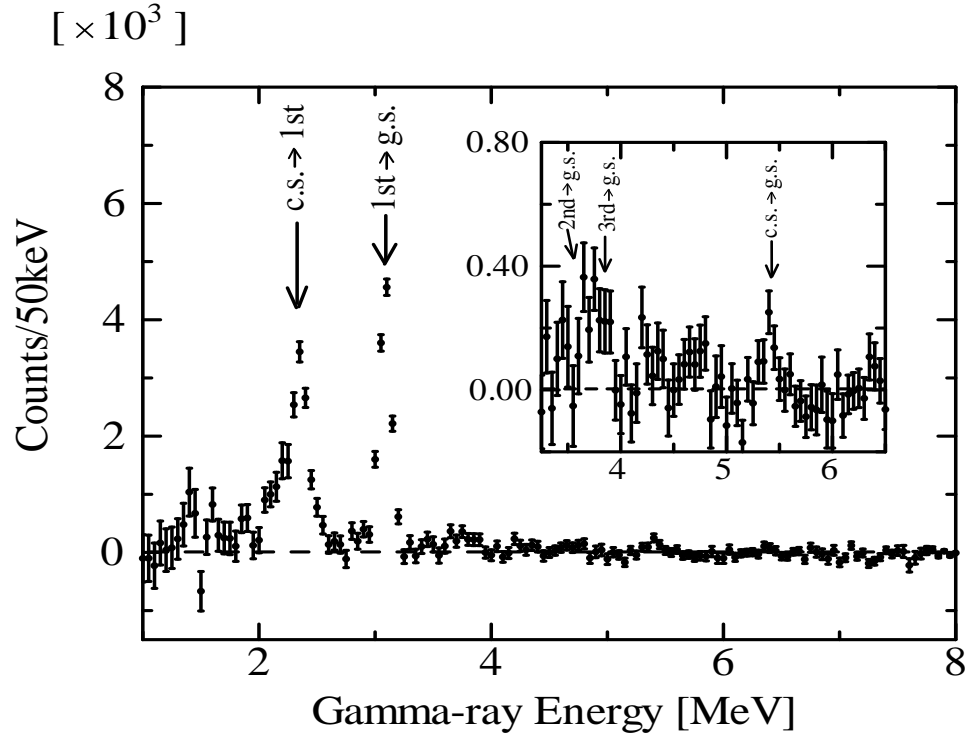


FIG. 5. Net  $\gamma$ -ray spectrum for the  $^{12}\text{C}(n, \gamma)^{13}\text{C}$  reaction. This spectrum was obtained by subtracting the  $\gamma$ -ray spectrum measured without the C sample from the background subtracted spectrum shown in 4.

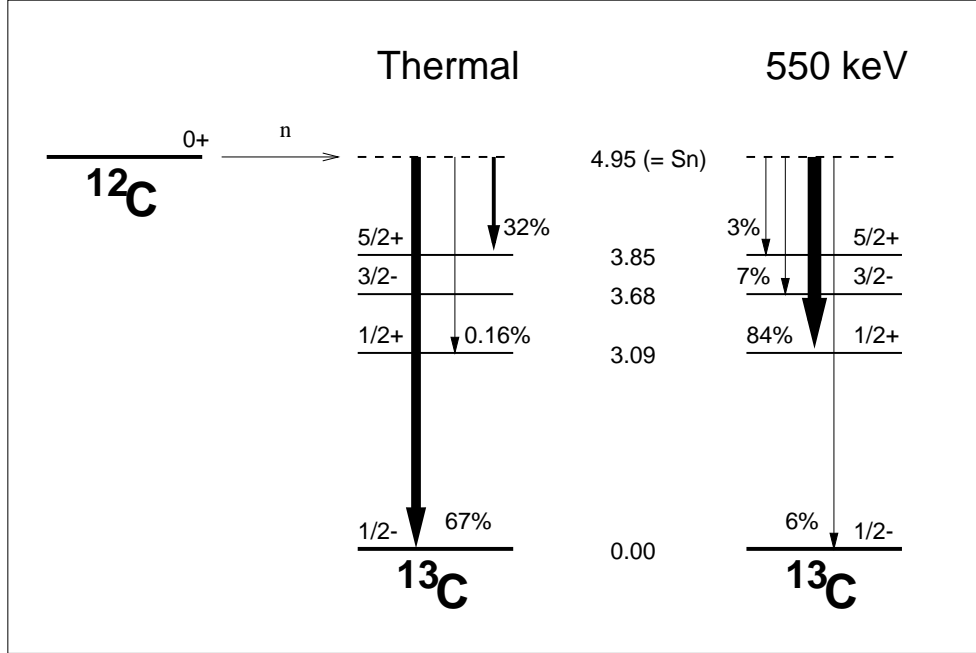


FIG. 6. Partial level scheme of  $^{13}\text{C}$ . The capture  $\gamma$ -ray branching ratios for incident thermal neutrons (left) and for the fast, 550 keV neutrons (right) are shown together with the excitation energies (in MeV).

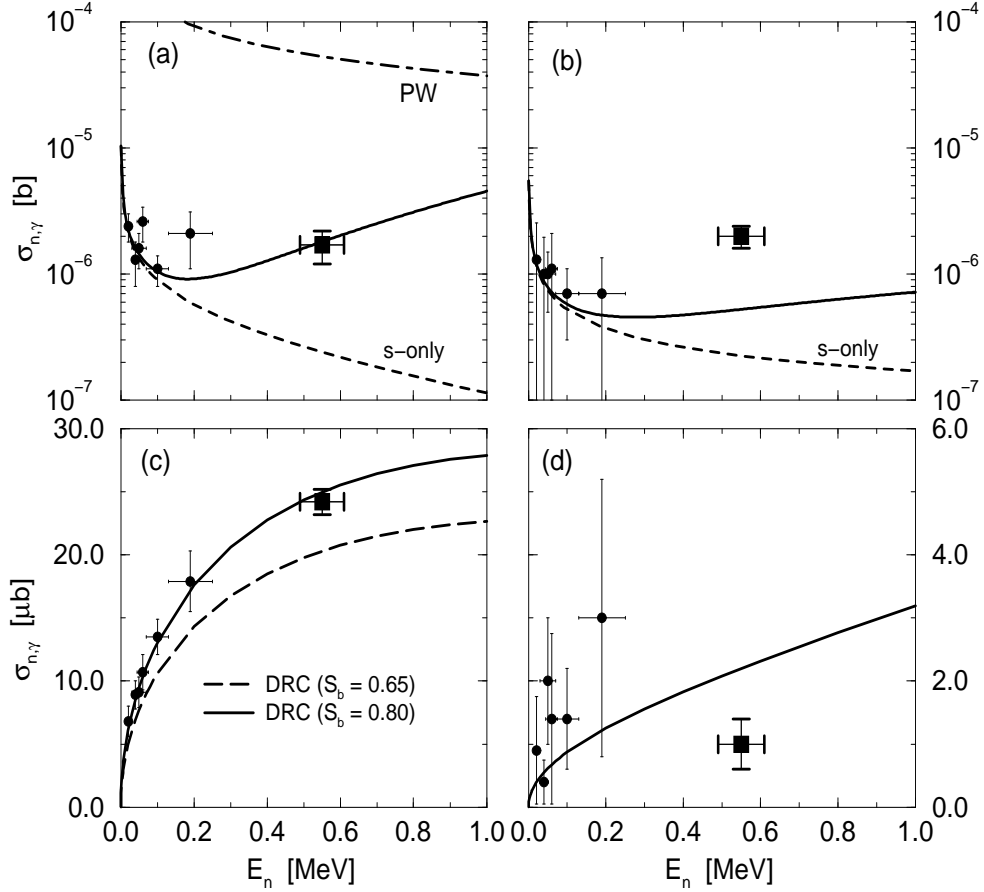


FIG. 7. Neutron capture cross section of  $^{12}\text{C}$  for (a) transitions leading to the  $^{13}\text{C}$  ground-state, (b) to the second-excited, (c) to the first-excited state and (d) to the third-excited state. In (a) and (b) the dashed line indicates the incident  $s$ -wave contribution only and the full line the total ( $s+d$ -wave) DRC. In (a), the line labelled with PW indicates a calculation made with a plane-wave wave function (see [6] for details). In (c), the dashed line indicates the result obtained using a spectroscopic factor  $S_b = 0.65$  whereas the full line indicates the result obtained using  $S_b = 0.80$ . The experimental values for  $E_n = 550$  keV (square symbols) are from the present experiment while the other experimental values are from a previous experiment [2].

# <sup>12</sup>C processing

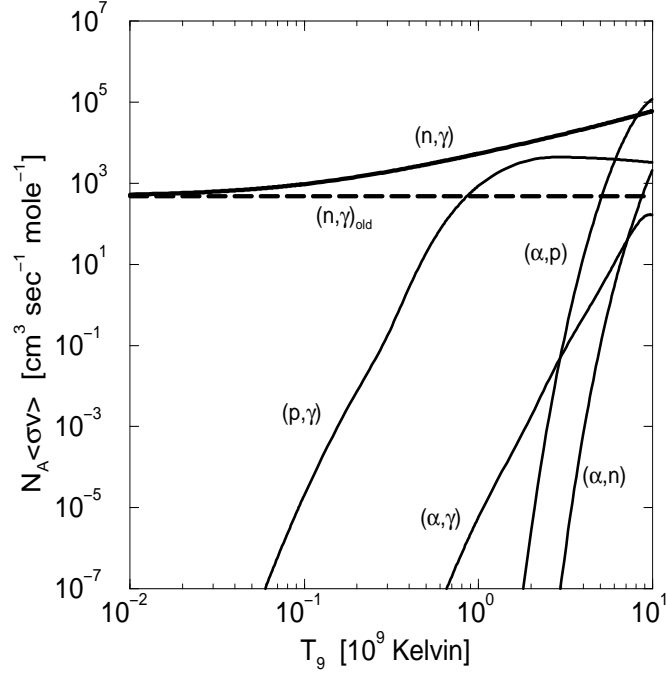


FIG. 8. The reaction rates for processing  $^{12}\text{C}$  from various reaction channels for temperatures ranging from  $10^7$  to  $10^{10}$  °K ( $T_9 \equiv 10^9$  °K). Except for the  $(n, \gamma)$  rate, the rates are from the Nuclear Astrophysics Data Service [21]. The dashed line, labelled by  $(n, \gamma)_{\text{old}}$ , corresponds to a neutron capture cross section  $\sigma_{n, \gamma}^{th} = 3.53$  mb and based on  $s$ -wave capture only. The increase with temperature of the neutron capture rate is due to the  $p$ - and  $d$ -wave DRC process. See text for details.



# TABLES

TABLE I. Correction factors for  $s$ - and  $p$ -wave neutrons.

Sample		$C_{nm}$	$C_{ns}$	$C_{nm} \times C_{ns}$
C	$s$ -wave	1.87	0.68	1.27
	$p$ -wave	1.65	0.68	1.13
Au	$s$ -wave	1.07	0.98	1.05

TABLE II. Measured and calculated capture cross sections ( $\mu\text{barn}$ ) at  $E_n^{lab} = 550$  keV.

Bound-state $E_x$ (MeV)	$E_\gamma$ (MeV)	$\sigma_{n,\gamma}^{exp}$ ( $\mu\text{barn}$ )	$\sigma_{n,\gamma}^{DRC}$ ( $\mu\text{barn}$ )
0.0	5.45	$1.7 \pm 0.5$	1.8
3.09	2.36	$24.2 \pm 1.0$	25.0 <sup>a</sup>
3.68	1.77	$2.0 \pm 0.4$	0.5
3.85	1.60	$1.0 \pm 0.4$	2.2

<sup>a</sup>Obtained using  $S_b = 0.80$ .

## FIGURE CAPTIONS

- FIGURE 1: Neutron energy spectrum measured by a  ${}^6\text{Li}$ -glass scintillation counter with a TOF method. The spectrum has been corrected for the energy-dependent neutron detection efficiency of the  ${}^6\text{Li}$ -glass.
- FIGURE 2: Time-of-flight spectrum measured by the NaI(Tl) detector for the Au sample. The sharp peak at channel 440 is due to the  $\gamma$ -ray from the  ${}^7\text{Li}(p, \gamma){}^8\text{Be}$  reaction. The regions F and B were chosen to obtain the foreground and background  $\gamma$ -ray spectra, respectively (see text).
- FIGURE 3: Foreground (solid line) and background (dotted line)  $\gamma$ -ray spectra for the  ${}^{12}\text{C}(n, \gamma){}^{13}\text{C}$ . Iron was used to cover the NaI(Tl) spectrometer.
- FIGURE 4: Background subtracted  $\gamma$ -ray spectra for the  ${}^{12}\text{C}(n, \gamma){}^{13}\text{C}$  reaction.
- FIGURE 5: Net  $\gamma$ -ray spectrum for the  ${}^{12}\text{C}(n, \gamma){}^{13}\text{C}$  reaction. This spectrum was obtained by subtracting the  $\gamma$ -ray spectrum measured without the C sample from the background subtracted spectrum shown in 4.
- FIGURE 6: Partial level scheme of  ${}^{13}\text{C}$ . The capture  $\gamma$ -ray branching ratios for incident thermal neutrons (left) and for the fast, 550 keV neutrons (right) are shown together with the excitation energies (in MeV).
- FIGURE 7: Neutron capture cross section of  ${}^{12}\text{C}$  for (a) transitions leading to the  ${}^{13}\text{C}$  ground-state, (b) to the second-excited, (c) to the first-excited state and (d) to the third-excited state. In (a) and (b) the dashed line indicates the incident  $s$ -wave contribution only and the full line the total ( $s+d$ -wave) DRC. In (a), the line labelled with PW indicates a calculation made with a plane-wave wave function (see [6] for details). In (c), the dashed line indicates the result obtained using a spectroscopic factor  $S_b = 0.65$  whereas the full line indicates the result obtained using  $S_b = 0.80$ .

The experimental values for  $E_n = 550$  keV (square symbols) are from the present experiment while the other experimental values are from a previous experiment [2].

- FIGURE 8: The reaction rates for processing  $^{12}\text{C}$  from various reaction channels for temperatures ranging from  $10^7$  to  $10^{10}$  °K ( $T_9 \equiv 10^9$  °K). Except for the  $(n, \gamma)$  rate, the rates are from the Nuclear Astrophysics Data Service [21]. The dashed line, labelled by  $(n, \gamma)_{old}$ , corresponds to a neutron capture cross section  $\sigma_{n,\gamma}^{th} = 3.53$  mb and based on  $s$ -wave capture only. The increase with temperature of the neutron capture rate is due to the  $p$ - and  $d$ -wave DRC process. See text for details.